This is an open access article published under an ACS AuthorChoice License, which permits copying and redistribution of the article or any adaptations for non-commercial purposes.

JCTC Journal of Chemical Theory and Computation

Article

pubs.acs.org/JCTC

Effect of Anharmonicity on Adsorption Thermodynamics

GiovanniMaria Piccini* and Joachim Sauer

Institut für Chemie, Humboldt Universität zu Berlin, Unter den Linden 6, 10099 Berlin, Germany

Supporting Information

ABSTRACT: The effect of anharmonic corrections to the vibrational energies of extended systems is explored. Particular attention is paid to the thermodynamics of adsorption of small molecules on catalytically relevant systems typically affected by anharmonicity. The implemented scheme obtains one-dimensional anharmonic model potentials by distorting the equilibrium structure along the normal modes using both rectilinear (Cartesian) or curvilinear (internal) representations. Only in the latter case, the modes are decoupled also at higher order of the potential and the thermodynamic functions change in the expected directions. The method is applied to calculate *ab initio* enthalpies, entropies, and Gibbs free energies for the adsorption of methane in acidic chabazite (H−CHA) and on MgO(001) surface. The values obtained for the adsorption of methane in H−CHA (273.15 K, 0.1 MPa, $\theta = 0.5$) are $\Delta H = -19.3$, $-T\Delta S = 11.9$, and $\Delta G = -7.5$ kJ/mol. For methane on the MgO(001) (47 K, 1.3×10^{-14} MPa, $\theta = 1$) $\Delta H = -14.4$, $-T\Delta S = 16.6$, and $\Delta G = 2.1$ kJ/mol are obtained. The calculated desorption temperature is 44 K, and the desorption prefactor is 4.26×10^{12} s^{-1}. All calculated results agree within chemical accuracy limits with experimental data.

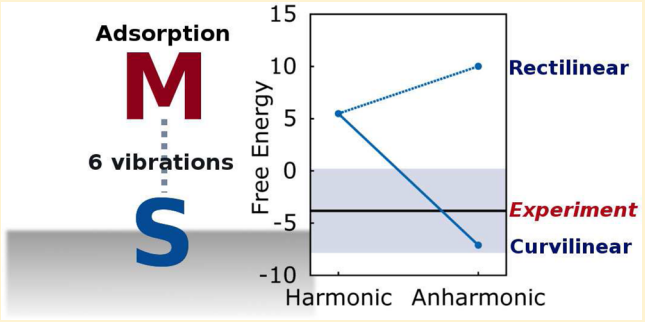

INTRODUCTION

Substantial progress has been made in the ab initio calculation of reaction energies and energy barriers for large chemical systems such as enzymes,[1] zeolite catalysts,[2−6] or metal−organic frameworks[7,8] with chemical accuracy. Such calculations combine high level quantum chemical calculations for the reaction site with low level calculations of the periodic structure, either using force fields[1] or density functional theory (DFT).[2−4,9] Unfortunately, free energy differences (i.e., entropies) cannot be calculated with the same accuracy using this approach.[10] However, understanding the role of entropy in adsorption processes is fundamental in catalysis and surface science.[11] The accurate ab initio calculation of such quantities represents a major challenge in computational biochemistry[12,13] and material science.[14,15] Usually, reliable force fields are available for biomolecular systems even for the reaction site allowing an extensive use of sampling schemes such as umbrella sampling[16] or thermodynamic integration.[17,18] Whereas many of these force fields are available for biological systems providing reliable descriptions of the potential energy surface (PES), this is not the case for molecule−surface interactions, especially if they involve active sites with a large periodic cell. Therefore, the calculation of entropy contributions from vibrational partition functions evaluated in the harmonic approximation has become a standard tool in evaluating rate constants for surface reactions[3] and free energies of adsorption.[8,10,19−21]

The harmonic oscillator model faces many limits especially for the low frequency modes arising from molecule−surface interactions and *soft* vibrational modes of the crystals as outlined in detail in a previous publication[14] (see also ref 22, section 10.5.2). To overcome these problems the authors suggested a computational protocol[14] which consists of an accurate structural refinement using an optimization in normal mode coordinates[23,24] followed by an accurate calculation of the harmonic frequencies including anharmonic corrections.[25] The present work deals with anharmonic corrections to the thermodynamic functions with particular attention to the derivation of the anharmonic model potential. As pointed out by Njegic and Gordon[26] the main reason for the failure of anharmonic corrections using the vibrational self-consistent field approach arises from the way the PES is sampled. The present approach takes only diagonal anharmonicity into account, i.e., to get the model potential the PES is sampled along the normal modes of vibration. In describing low frequency/high amplitude motions, e.g., in weakly bound systems,[27,28] rectilinear normal mode displacements (linear combinations of Cartesian coordinates) are not sufficient and they result in an artificial large coupling of many vibrational coordinates. Njegic and Gordon suggested to improve the sampling of the PES by employing curvilinear normal mode displacements defined using internal coordinates. They have shown[26] that this approach has a strong effect on the thermodynamics of formation of some simple molecular systems such as the water dimer or sulfuric acid.

In this work the sampling scheme in curvilinear normal mode displacements is adapted to treat anharmonicity in extended

Received: April 4, 2014
Published: May 22, 2014

Downloaded via RWTH AACHEN HOCHSCHUL BIBL on January 31, 2024 at 12:22:40 (UTC).
See https://pubs.acs.org/sharingguidelines for options on how to legitimately share published articles.

 © 2014 American Chemical Society dx.doi.org/10.1021/ct500291x | J. Chem. Theory Comput. 2014, 10, 2479−2487

systems in order to get entropy estimates with chemical accuracy. The definition of internal coordinates for periodic systems, i.e. including periodic images in the definition of the topology, has been discussed in different works.[29−31] The present work uses the definition of periodic redundant internal coordinates proposed by Bucko et al.[31] due to its completeness in defining intra and inter cell bonds.

The proposed protocol is applied to two relevant systems. In the first case, molecular adsorption of methane in acidic chabazite[32] is a model system for catalysis and sorption in microporous materials.[32−38] An accurate prediction of the adsorption energy and entropy for such a process is key to understanding its underlying nature and, further on, to design more efficient materials. The second case, molecular adsorption of a monolayer ($\theta = 1$) of methane on the MgO(001) surface, is a prominent model system of surface science.[39−45] It is particularly interesting since almost the total adsorption energy is due to dispersion, and the stability of the adsorption complex is not only coming from molecule−surface interaction but also from the lateral interaction of the molecules in the monolayer.[45] Due to the particular structure and interactions of the molecules in the monolayer single molecular translational and rotational contributions combine into collective hindered translational and rotational motion of the whole layer making this system particularly affected by anharmonicity. Theoretical results can be compared with accurate experimental results obtained by Tait et al.[39]

METHODS

In this section the concept of normal modes of vibration and the variational approach adopted by the authors in the previous work[14] to calculate anharmonicity is recalled. Most of the attention will be paid to the techniques for sampling the PES to get accurate anharmonic model potentials.

Normal Modes of Vibration. For a generic molecular system, the vibrational Hamiltonian can be written in harmonic approximation as

$$\mathbf{H} = \frac{1}{2}(\mathbf{\Delta\dot{x}}^{\mathrm{T}}\mathrm{M}\mathbf{\Delta\dot{x}} + \mathbf{\Delta x}^{\mathrm{T}}\mathbf{H}\mathbf{\Delta x}) \tag{1}$$

where $\mathbf{\Delta x}$ is the vector of the Cartesian atomic displacements from the equilibrium position, $\mathbf{M}$ is the diagonal matrix of atomic masses ($M_{ij} = \delta_{ij}m_i$), $\mathbf{H}$ is the energy Hessian, i.e., the harmonic force constant, matrix. Index i goes from 1 to $3N$ counting each Cartesian $\{x, y, z\}$ degree of freedom per atom. Introducing mass-weighted coordinates $\mathbf{q} = \mathbf{M}^{1/2}\mathbf{\Delta x}$, the Hamiltonian transformes into

$$\mathbf{H} = \frac{1}{2}(\mathbf{\dot{q}}^{\mathrm{T}}\mathbf{\dot{q}} + \mathbf{q}^{\mathrm{T}}\mathbf{fq}) \tag{2}$$

where $\mathbf{f}$ is the mass-weighted Hessian matrix. Normal mode coordinates $\mathbf{Q}$ are defined as linear combination of mass-weighted coordinates

$$\mathbf{Q} = \mathbf{s}^{\mathrm{T}}\mathbf{q} \tag{3}$$

Imposing the orthogonality of the matrix $\mathbf{s}$ and defining a similarity transformation of the Hessian

$$\mathbf{s}^{\mathrm{T}}\mathbf{s} = 1,\ \mathbf{s}^{\mathrm{T}}\mathbf{fs} = \mathbf{F}, \quad \text{where } F_{ij} = \delta_{ij}\omega_i^{\,2} \tag{4}$$

the Hamiltonian can be written in diagonal from

$$\mathbf{H} = \sum_{i=1}^{3N} \frac{1}{2}(\dot{Q}_i^{\,2} + \omega_i^{\,2}Q_i) \tag{5}$$

Thus, a linear transformation between Cartesian and normal mode coordinates is defined

$$\mathbf{\Delta x} = \mathbf{M}^{-1/2}\mathbf{q} = \mathbf{M}^{-1/2}\mathbf{sQ} = \mathbf{SQ} \tag{6}$$

The resulting transformation matrix $\mathbf{S}$ is a matrix of eigenvectors $[\mathbf{v}_1, \mathbf{v}_2, ..., \mathbf{v}_{3N}]$ where each column corresponds to the Cartesian coefficients of the linear combination for the kth normal mode. Thus, it is possible to displace the atoms along a specific normal mode independently.

Quantum Diagonal Anharmonicity. The aim is to solve the Schrödinger equation variationally for all the normal modes independently in a basis of harmonic functions with a sixth-order model potential. The Hamiltonian for a generic kth mode is

$$H = -\frac{\hbar^2}{2}\frac{\mathrm{d}^2}{\mathrm{d}Q_k^{\,2}} + a_0 + a_1Q_k + a_2Q_k^{\,2} + a_3Q_k^{\,3} + a_4Q_k^{\,4} + a_5Q_k^{\,5} + a_6Q_k^{\,6} \tag{7}$$

with Q_k being the normal coordinate of the mode and a_i ($i = 0$, ..., 6) as the polynomial fitting coefficients of the potential. The Hamiltonian matrix elements

$$H_{mn} = \langle\varphi_m|H|\varphi_n\rangle \tag{8}$$

are defined with the harmonic functions ϕ_m which are solutions of the one-dimensional quantum harmonic oscillator

$$\varphi_m = \sqrt{\frac{1}{2^m m!}}\left(\frac{\omega_k}{\pi\hbar}\right)^{1/4} e^{-\omega_k/2\hbar Q_k^{\,2}}\mathcal{H}_m\left(\sqrt{\frac{\omega_k}{\hbar}}\,Q_k^{\,2}\right) \tag{9}$$

with $m = 0, 1, ...$ and $\mathcal{H}_m$ being the mth order Hermite polynomial. After application of Hermite polynomial rules to eq 8, the matrix elements can be derived analytically (see the Supporting Information (SI)).

Diagonalization of the Hamiltonian matrix for a certain number of harmonic basis functions yields the eigenvalues ϵ_i of the energy states of the anharmonic oscillator. The quantum anharmonic vibrational partition function is approximated as a sum over the states

$$q_a = \sum_{i=0}^{\infty} \mathrm{e}^{-\epsilon_i/k_{\mathrm{B}}T} \approx \sum_{i=0}^{m} \mathrm{e}^{-\epsilon_i/k_{\mathrm{B}}T} \tag{10}$$

Its convergence with respect of the number of states, given by the number of harmonic oscillator functions ($\Delta q_a = q_a^m - q_a^{m-1} < \sigma$, where σ is a reasonably small number), is used as a variational criterion. This condition is combined with the convergence of the fundamental anharmonic frequency of the oscillator $\Delta\nu_a = \nu_a^m - \nu_a^{m-1} < \delta$, where $\nu_a = (\epsilon_1 - \epsilon_0)/h$ (h here is the Planck's constant). When converged, the energy states are used to calculate internal energies and entropies from the direct sum over states (see the SI).

Sampling of the PES. To get the model potential of eq 7 the PES has to be sampled along each normal mode. Having the transformation of eq 6 the structure can be distorted along the normal modes in Cartesian coordinates as previously done:[14,25]

$$\mathbf{x}_k^{\mathrm{disp}} = \mathbf{x}_0 \pm P\ \mathrm{d}Q_k^{\mathrm{disp}}\mathbf{v}_k \tag{11}$$

dx.doi.org/10.1021/ct500291x | J. Chem. Theory Comput. 2014, 10, 2479−2487

The integer P runs from 1 to n_{grid} that is the number of symmetric grid points used to sample the PES, dQ_k^{disp} is the entity of the displacement defined as $dQ_k^{disp} = 4/2\pi\omega_k{}^{1/2}2n_{grid}$ which ensures that the wave function decays to zero at the furthest points (classical turning points of the harmonic oscillator),[46] and $\mathbf{v}_k$ is the eigenvector of the kth mode and $\mathbf{x}_0$ is the equilibrium structure. However, as reported in detail by Njegic and Gordon,[26,46] normal mode distortions in Cartesian coordinates are rectilinear by definition; therefore they do not preserve any internal coordinate. Thus, the diagonal potential does not directly correspond to a stretch, bend, or torsion but rather to a mixture of all these internal coordinates. For high frequency vibrations which have low vibrational amplitudes linear (Cartesian) displacements are still a good approximation for a correct sampling of the PES. However, for low frequency/high amplitude vibrations linear displacements result in an artificial coupling of all vibrations therefore the sampling does not catch the correct PES. Since stretching modes are linear by construction they are in general not affected by such problems whereas bends and torsion are linear for infinitesimal displacements only.[47,48] This work follows Boatz and Gordon[49] in defining a Wilson transformation of the normal modes in internal coordinates. The well-known B-matrix[47] gives the relationship between Cartesian displacement coordinates and internal coordinates

$$\mathbf{\Delta R} = \mathbf{B\Delta x} \quad \text{where } B_{i,j} = \frac{\partial R_i}{\partial x_j} \tag{12}$$

Simple internal coordinates are defined as stretching, bends and torsions and the dimension of their space can vary from $3N - 6$, $3N - 5$, or $3N - 3$ for a nonlinear, linear, and periodic system, respectively (nonredundant set) up to a specific number Ω (redundant set). The use of the latter set is critical for a proper description of the vibrational modes as also suggested by Boatz and Gordon[49] and others.[50−55] Independently of the choice of the internal coordinates the Cartesian Hessian matrix can be transformed into internals as

$$\mathbf{\Phi} = (\mathbf{B}^{-1})^{\mathrm{T}}\mathbf{H}(\mathbf{B}^{-1}) \text{ and vice versa} \quad \mathbf{H} = \mathbf{B}^{\mathrm{T}}\mathbf{\Phi B} \tag{13}$$

where $\mathbf{\Phi}$ is the Hessian matrix in internal coordinates. From the definition of the diagonal Hessian of eqs 4 and 6

$$\mathbf{S}^{\mathrm{T}}\mathbf{HS} = \mathbf{F}, \quad \text{where } \mathbf{S} = \mathbf{M}^{-1/2}\mathbf{s} \tag{14}$$

and substituting the Cartesian Hessian (eq 13) it follows that

$$\mathbf{F} = \mathbf{S}^{\mathrm{T}}(\mathbf{B}^{\mathrm{T}}\Phi\mathbf{B})\mathbf{S} = \mathbf{D}^{\mathrm{T}}\mathbf{\Phi D} \tag{15}$$

where the matrix

$$\mathbf{D} = \mathbf{BS} \tag{16}$$

is the matrix of normal mode eigenvectors $[\gamma_1, \gamma_2, ..., \gamma_{3N}]$. Column k refers to the kth mode and contains the linear combination coefficient for the internal coordinates. Having these eigenvectors the Cartesian equilibrium geometry can be distorted along each normal mode by a displacement $\boldsymbol{\sigma} = P\, dQ_k^{disp}\gamma_k$

$$\mathbf{x}_k^{disp} = \mathbf{x}_0 \pm (\mathbf{B}^{-1})^{\mathrm{T}}\boldsymbol{\sigma}_k \tag{17}$$

Since by construction internal coordinates are nonlinear (curvilinear), the above equation must be solved iteratively as is well-documented in the literature.[48,56−58] From the new Cartesian coordinates of eq 17 a new set of internal coordinates is calculated as $\mathbf{\Delta R}_n = \boldsymbol{\sigma}_k - (\mathbf{R}_n - \mathbf{R}_0)$ where n is the iteration counter. The quantity $\mathbf{\Delta R}_n$ represent the difference between the desired displacement in internal coordinates $\boldsymbol{\sigma}_k$ and the actual one during the iterative back-transformation. The latter is then used to calculate a new Cartesian geometry $\mathbf{x}_{k,n+1}^{disp} = \mathbf{x}_{k,n}^{disp} + (\mathbf{B}^{-1})^{\mathrm{T}}\mathbf{\Delta R}_n$. The iteration is looped until $(\mathbf{B}^{-1})^{\mathrm{T}}\mathbf{\Delta R}_n < 10^{-6}$ or if $n > 25$. In some cases, the iteration might diverge during the refinement, therefore if $\mathbf{\Delta R}_n > \mathbf{\Delta R}_1$ the procedure is stopped and Cartesian geometry is reverted to the first estimate $\mathbf{x}_1^{disp}$. While in general such a procedure is acceptable in structure optimizations, it might be source of severe accuracy problems when trying to sample the PES. A proper choice of the internal coordinates has proven to be essential to ensure convergence of the transformation.

A last remark must be spent on the definition of the inverse of the B-matrix. Since in general the B-matrix is rectangular no direct inverse matrix can be calculated. To calculate the inverse several methods have been proposed.[49,58,59] The derivation employed in this work follows the indications of Boatz and Gordon[49] and Pulay and Fogarasi.[59] The goal is to remove the redundancies of $\mathbf{B}$ which are the linearly dependent rows of the matrix. A squared $\mathbf{G}$ matrix (also know as the Wilson G-matrix) is defined as

$$\mathbf{G} = \mathbf{BM}^{-1}\mathbf{B}^{\mathrm{T}} \tag{18}$$

where $\mathbf{M}^{-1}$ is the inverse of the atomic mass matrix defined above. The eigenvalue equation of $\mathbf{G}$

$$\mathbf{G}(\mathbf{K} \quad \mathbf{L}) = (\mathbf{K} \quad \mathbf{L})\begin{pmatrix}\mathbf{\Lambda} & \mathbf{0}\\ \mathbf{0} & \mathbf{0}\end{pmatrix} \tag{19}$$

has $3N - m$ (m = 6, 5, 3) *nonzero* eigenvalues associated with the submatrix $\mathbf{K}$ and $\Omega - (3N - m)$ zero eigenvalues associated with the submatrix $\mathbf{L}$ corresponding to the redundancies. Therefore, the matrix is singular and cannot be inverted directly. The generalized inverse of the matrix $\mathbf{G}$ is obtained from eq 19 as

$$\mathbf{G}^{-1} = (\mathbf{K} \quad \mathbf{L})\begin{pmatrix}\mathbf{\Lambda}^{-1} & \mathbf{0}\\ \mathbf{0} & \mathbf{0}\end{pmatrix}\begin{pmatrix}\mathbf{K}^{\mathrm{T}}\\ \mathbf{L}^{\mathrm{T}}\end{pmatrix} \tag{20}$$

transforming it to diagonal form and inverting only the *nonzero* eigenvalues. Therefore, taking the inverse of both sides of eq 18

$$\mathbf{G}^{-1} = (\mathbf{BM}^{-1}\mathbf{B}^{\mathrm{T}})^{-1}$$

$$\mathbf{G}^{-1} = (\mathbf{B}^{-1})^{\mathrm{T}}\mathbf{MB}^{-1} \tag{21}$$

the expression for the generalized inverse of the B-matrix is obtained

$$\mathbf{B}^{-1} = \mathbf{M}^{-1}\mathbf{B}^{\mathrm{T}}\mathbf{G}^{-1} \tag{22}$$

When treating large systems with many redundancies the calculation and subsequent inversion of $\mathbf{G}$ can be computationally demanding. Having this expression for the inverse B-matrix it can be used in the procedure for the internal to Cartesian coordinates back-iteration.

COMPUTATIONAL DETAILS

Calculation of harmonic frequencies in normal mode coordinates and fit of the PES to a sixth order polynomial was implemented in the program EIGEN_HESS_ANHARM_INT. The program is a modified version of EIGEN_HESS_ANHARM.[14] Both programs are written in F90 and interface with VASP[60] to get total energies and gradients from single

point calculations. The calculation of the internal coordinates and relative B-matrix are performed using the Python script WriteBmatrix.py by Tomas Bučko which allows the variation of the covalent and van der Waals radii to get different internal coordinate sets. For all the systems described in this work each plane wave DFT calculation has been performed using a 600 eV energy cutoff requiring an energy difference between two consecutive SCF cycles of 10^{-8} eV/cell. The PBE[61] functional has been employed and Grimme's "D2" parameters[62] are used to include dispersion interactions.[63] Thermodynamic properties such as translational, rotational, harmonic, and anharmonic energies and entropy contributions were obtained using the local F90 program THERMO.

CH_4 in H−CHA. The gas phase calculation of the methane molecule has been performed putting it in a cubic cell of 15 Å × 15 Å × 15 Å. The supercell of dimensions a = 18.90 Å, b = 9.44 Å, c = 9.29 Å, with α = 94.0051°, β = 94.8903°, γ = 95.3793° for acidic chabazite contains two active sites (See Figure 1). This

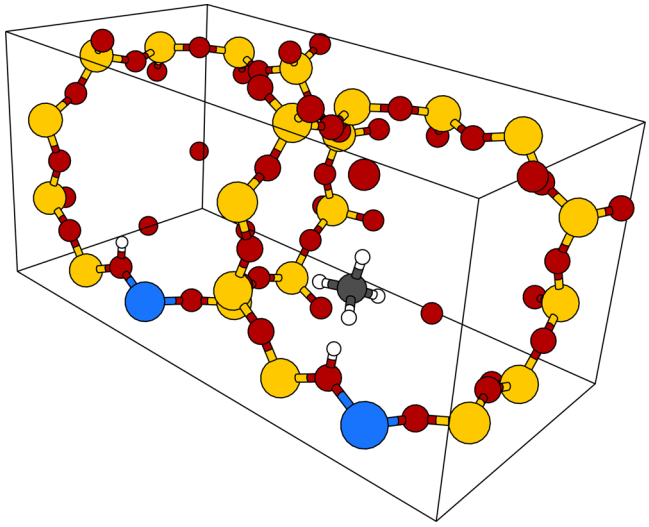

Figure 1. H−CHA 2a supercell showing the adsorption complex of the methane molecule at the acidic hydrogen in position O2 (oxygen shared by two eight-membered rings and one four-membered). Color key: yellow—silicon, red—oxygen, blue—aluminum, gray—carbon, and white—hydrogen.

has been obtained doubling the triclinic unit cell along the lattice vector a. At half coverage (θ = 0.5), this ensures a negligible lateral interaction between adsorbed molecules and allows a Γ-point only calculations for a proper electronic structure convergence. The Al/Si ratio for this zeolite is 1/11.

CH_4 on MgO(001). The gas phase calculation of the methane molecule has been performed for an orthorhombic supercell of 8.42 Å × 8.42 Å × 25.00 Å. To model the adsorption of methane on the MgO(001) surface the "ROT" structure[40] has been adopted which was also considered by Tosoni and Sauer.[45] It consists of a slab of three layers of magnesium oxide where at each side surface four methane molecules are adsorbed (See Figure 2). Th surface is a 2a × 2a supercell formed by three layers of MgO. The 2 × 2 double cell is mandatory to accommodate the methane molecules in this particular arrangement. The dimensions of the orthorhombic unit cell are 8.42 Å × 8.42 Å × 25.00 Å. The size of the c lattice parameter ensures enough vacuum to avoid artificial interactions between the periodic images. The reciprocal space has been sampled using a Monkhort−Pack grid[64] of 2

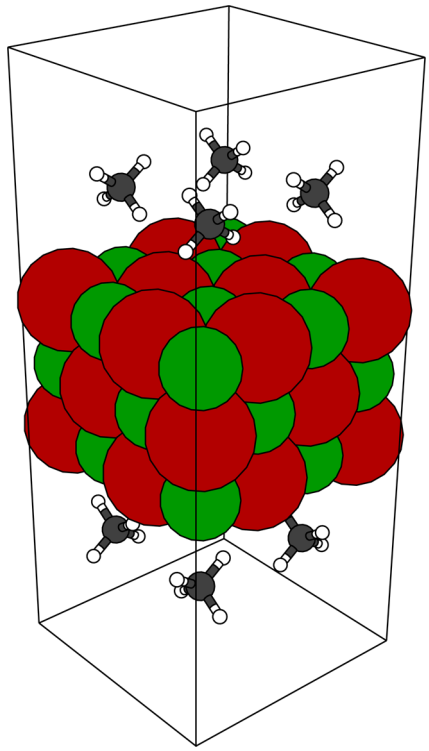

Figure 2. Slab model for methane adsorption on MgO(100) surface proposed by Tosoni and Sauer[45] showing the double monolayer structure on each side of the slab. Color key: green—magnesium, red—oxygen, gray—carbon, and white—hydrogen.

× 2 × 1 k-points. To describe properly the dispersion interactions for Mg^{2+} ions the Grimme parameters for Ne have been used (c_6 = 0.63 and R_6 = 1.243).[45] In ref 45, Tosoni and Sauer have derived parameters for Mg^{2+} following the Grimme protocol and obtained results that are very close to Ne parameters,[45] which did not come as a surprise because the number of valence electrons is the same for both Mg^{2+} and Ne.

RESULTS AND DISCUSSION

CH_4 in H−CHA. Figure 1 shows the cell of H−CHA loaded with methane. The adsorption complex considered has been preoptimized using the conjugate-gradient algorithm implemented in VASP and subsequently refined using the normal-mode optimization.[14] The reference structure is the same as described in ref 14. Starting from the Cartesian Hessian obtained using the finite differences algorithm of VASP, Cartesian eigenvectors (normal modes) have been derived. The latter have been transformed into internal coordinates as described in the Methods section. To get consistent results anharmonic corrections have been applied to the vibrations of the adsorption complex, the unloaded chabazite and the methane molecule. Due to the particular *soft* vibrational structure of zeolites,[65−68] large amplitude motions not only occur for the molecule−active site vibrations but also for the crystal framework modes. Therefore, the description of normal modes in terms of internal coordinates is mandatory to sample the PES correctly. For each vibrational mode, a new set of accurate harmonic frequencies have been calculated using distortions of the normal mode in internal coordinates. Eight symmetric points are used and the Fornberg formulas[69] are applied. As previously,[14] having this accurate sampling, the PES can be fit to a 6th-order polynomial and used to calculate

anharmonic frequencies for all modes and thermodynamic functions.

To get an accurate estimate of the internal energy and enthalpy, the energy at the minimum of the PES has been obtained using the hybrid MP2:PBE + ΔCCSD(T) method proposed by Tuma and Sauer,[70,71] while ZPVE (zero point vibrational energy) and thermal enthalpy contributions are calculated using the vibrations for the PBE+D potential energy surface. Table 1 shows the final energy estimate[72] and compares

Table 1. Electronic Adsorption Energy for Adsorption of Methane in H−CHA from MP2:PBE + ΔCCSD(T), PBE+D, PBE, and Dispersion (D)[a]

	method[b]	ΔE_e
Tuma and Sauer[72]	hybrid MP2:PBE + ΔCCSD(T)	−29.4
	PBE+D	−34.8
this work	PBE//PBE+D	−8.2
	D//PBE+D	−26.5

[a]All in kilojoules per mole. [b]"//" stands for "at the structure of".

it with the PBE+D results and its PBE and dispersion components. The hybrid MP2:PBE method which combines MP2 cluster models with PBE+D for periodic models yields an energy minimum structure, at which the effect of CCSD(T) is evaluated on smaller cluster models. For details of the method, see refs 45, 70, and 71, and for applications, see refs 2−4, 63, and 73.

Table 2 shows the thermodynamic functions for the adsorption of methane on acidic chabazite at standard

Table 2. Zero Point Corrected Energies, ΔE_0, Enthalpies, ΔH, Entropy Terms, $-T\Delta S$, and Gibbs Free Energies, ΔG, for Adsorption of Methane in H−CHA at Standard Conditions (273.15 K, 0.1 MPa, θ = 0.5)[a]

	harmonic			anharmonic		
	standard[b]	Cart[c]	NM[c]	anh-Cart[c]	anh-int[c]	exp (extrapol)[d]
ΔE_0	−25.1	−25.4	−24.6	−25.4	−22.9	
ΔH	−24.0	−26.3	−25.1	−30.2	−19.3	−16.7
$-T\Delta S$[e]	34.7	29.34	30.2	39.9	11.9	12.9
ΔG	10.7	3.1	5.1	9.7	−7.5	−3.8

[a]All in kilojoules per mole. [b]Reference structure optimized using VASP conjugate-gradients. [c]Reference structure optimized using normal mode coordinates. [d]Extrapolated from results for ethane and propane on H−CHA (Al/Si = 1/11).[74] [e]38.68 and 11.32 kJ/mol due to loss of translational and rotational degrees of freedom, respectively.

conditions (273.15 K, 0.1 MPa) for half coverage (θ = 0.5). The method "Standard" refers to the results obtained using VASP conjugate-gradient optimization and Cartesian harmonic analysis. Comparison is made with the results obtained after refining the structure with the normal mode optimizer and calculating the vibrational partition function using harmonic frequencies resulting from Cartesian distortions (Cart) or from normal mode distortions (NM). In addition, results are compared with anharmonic frequencies obtained from rectilinear (anh-Cart) or from curvilinear distortions (anh-int). Thermal contributions to the total energies are derived from the translational, rotational, and vibrational (harmonic and anharmonic) partition functions.

Figure 3 summarizes the results. The black solid line is the experimental value extrapolated from calorimetric data for

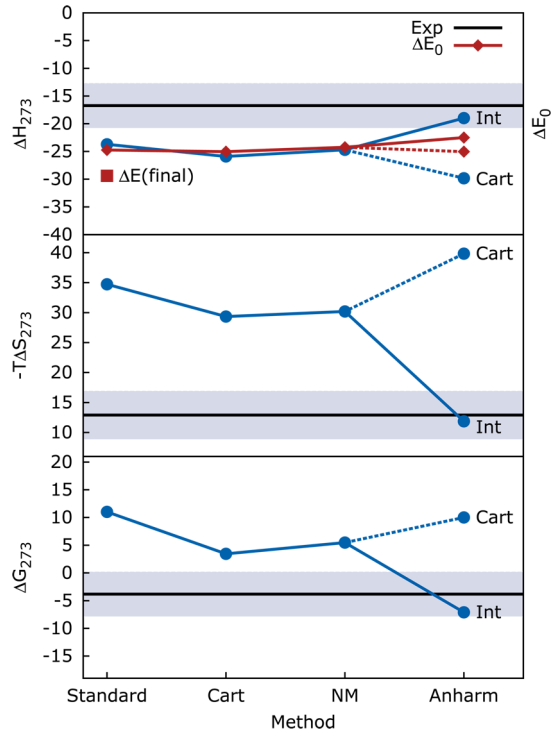

Figure 3. Enthalpies, ΔH, entropy, $-T\Delta S$, and Gibbs free energies, ΔG, for adsorption of methane in H−CHA at standard conditions (273.15 K, 0.1 MPa, θ = 0.5); all in kilojoules per mole.

ethane and propane adsorption on a sample of H−CHA (Al/Si = 1/11),[74] and the gray bar around it represents the chemical accuracy "region" (X_{Exp} ± 1 kcal/mol ≈ X_{Exp} ± 4 kJ/mol). The red full square is the MP2:PBE + ΔCCSD(T) adsorption energy.

The results show that the anharmonic corrections affect the thermodynamic functions significantly. Entropy is extremely sensitive to such changes in the vibrational structure. There is a large differences of almost 20 kJ/mol between the entropy term calculated using anharmonic frequencies with internal coordinate sampling (anh-int) and harmonic frequencies calculated in different ways (standard, Cart, NM). This illustrates the failure of the harmonic oscillator model in describing weak and noncovalent bonding of the nuclei. This breakdown can be explained by the specifics of the adsorption process. When the adsorption complex forms, the molecule looses its translational and rotational DOFs which are converted into vibrations. The translations and the rotations in the gas phase give to the system a higher entropy than resulting from the six molecule−surface vibrations. Therefore, adsorption is generally accompanied by a relatively high entropy loss. Describing the adsorption complex as a pure system of harmonic oscillators (especially for molecular- and physisorption) is definitely a rough approximation since the weak interactions of the molecule with the active site are far from being well-represented by a mass-spring model. The results is a fictitiously large entropy loss becoming unreasonable when the temperature of the system increases, i.e., when a strongly bound model for the adsorption complex becomes unrealistic.

dx.doi.org/10.1021/ct500291x | J. Chem. Theory Comput. 2014, 10, 2479−2487

Attention must be paid to the way the PES is sampled along the normal modes and the consequences that this can have on the thermodynamics.[26] The enthalpy and entropy differences between anh-int and anh-Cart are huge. The variational scheme proposed uses one-dimensional model potentials from a polynomial fit of the PES. As explained in the introduction, for large amplitude modes, rectilinear distortions are not able to preserve the internal coordinates of the system unless infinitesimal steps are used. The result is a fictitious coupling of all the modes. Therefore, the PES is not sampled along the normal mode only but receives contributions also from other coupled coordinates, and this results in a potential well that is narrower than the starting harmonic one. This is the reason why anharmonic contributions from rectilinear PES sampling yield higher frequencies and, thus, lower vibrational entropies of the adsorption complex. This is avoided when the normal modes are expressed in curvilinear coordinates. The anharmonic corrections obtained this way go in the right direction and are very close to the experimental values. The deviations for the enthalpy, the entropy term $-T\Delta S$, and the Gibbs free energy are with −2.6, −1.0, and −3.6 kJ/mol all within chemical accuracy limits.

A final remark concerns the choice of the sets of internal coordinates employed. In this work, simple internals are used to describe covalent bonds such as bond stretches, angle bends, and torsions, while for long-range interactions inverse power coordinates proposed by Baker and Pulay[57] are used. In most cases even a redundant set of coordinates obtained from the topology of the system using standard covalent and van der Waals radii is not complete enough to describe specific vibrational modes. It is possible then to scale the covalent and van der Waals radii in order to include more internals able to describe a specific motion. Unfortunately this procedure can not be easily generalized and the user must pay attention in selecting a proper set of internals for some specific modes. As an empiric rule, it has been observed for this specific case that hindered rotational modes are better described when the covalent radius is expanded by 20−30%. This way more bending and torsional coordinates are generated between the active site and the molecule able to describe the particular kind of motion. To describe more accurately hindered translational modes the van der Waals radius is expanded by 80−100% or more if needed. This partially ensures a proper motion of the adsorption complex keeping spurious contributions from other internal coordinates negligible. As mentioned, no general recipe can be applied to such problems and some chemical intuition is still needed to solve every specific case. Even for small molecular cases, a proper set of internals has to be chosen accurately case by case.[27,28] It is clear then that for large systems the control of the user is less, and many tests must be done in order to get an appropriate set. For some modes, the problems are pathological and anharmonicity cannot be meaningfully treated. In these cases simple harmonic frequencies are taken, but they are anyway a small minority in the whole set of frequencies.

CH_4 on MgO(001). Figure 2 shows the model unit cell for the methane monolayer on MgO(001). The use of rectilinear displacements is sufficient for sampling the PES of the normal mode vibrations of the bare MgO model surface. Nevertheless, particular attention must be paid to the choice of the set of redundant internal coordinates for the adsorption complex. The best choice proved to be a minimal set of valence type internal coordinates (i.e., 0% of covalent radii expansion) wheras the nonbonded type internal coordinates were determined expanding the van der Waals radii by 300% of their original values. This combination appeared to be the best compromise to describe both high frequency (intramolecular and crystal) modes and low frequency (intermolecular monolayer and surface) modes.

Also for this system the electronic energy difference at the minimum of the PES is taken from MP2:PBE+D + ΔCCSD(T) calculations of Tosoni and Sauer (Table 14 of ref 45). In Table 3, the PBE+D energy and the hybrid MP2:PBE+D + ΔCCSD(T) energy[45] are reported. This latter value is used for ΔE in this paper whereas all nuclear motion contributions refer to the PBE+D potential energy surface.

Table 3. Electronic Adsorption Energy for Adsorption of Methane on MgO(001) from MP2:PBE + ΔCCSD(T), PBE +D, PBE, and Dispersion (D)[a]

	method[b]	ΔE_e
Tosoni and Sauer[45]	MP2:PBE+D + ΔCCSD(T)	−13.3
	PBE+D	−14.7
this work	PBE//PBE+D	−1.3
	D//PBE+D	−13.4

[a]All in kilojoules per mole (per molecule). [b]"//" stands for "at the structure of".

Table 4 shows the thermodynamic functions related to the adsorption of a monolayer (θ = 1) of methane on the MgO(001) surface at desorption conditions (T = 47K, p = 1.3 × 10^{-14} MPa). The nomenclature is the same as for Table 2. The standard column is not present since no minimum (all real frequencies) was detected using standard optimization methods, conjugate-gradients in this case. Therefore, all the results reported refer to a minimum structure obtained by normal mode reoptimization[14] considering the whole set of eigenvalues and eigenvectors obtained from the previous harmonic analysis. The rational function optimization method ensures a downhill direction of the step toward the local minimum. Thermal contributions to the total energies are derived from the translational, rotational and vibrational (harmonic and anharmonic) partition functions.

Table 4. Zero Point Corrected Energies, ΔE_0, Enthalpies, ΔH, Entropy Terms, $-T\Delta S$, and Gibbs Free Energies, ΔG, for Adsorption of Methane on MgO(001) Surface at Experimental Desorption Conditions (47 K, 1.3 × 10^{-14} MPa, θ = 1)[a]

	harmonic		anharmonic		
	Cart[b]	NM[b]	anh-Cart[b]	anh-int[b]	exp[39]
ΔE_0	−9.7	−9.8	−12.5	−13.4	
ΔH	−10.7	−10.9	−13.7	−14.4	−12.2
$-T\Delta S$[c]	16.8	16.7	16.7	16.6	12.2[d]
ΔG	6.1	5.8	3.00	2.1	0.0[d]

[a]All in kilojoules per mole (per molecule). [b]Reference structure optimized using normal mode coordinates. [c]16.52 and 0.92 kJ/mol due to loss of translational and rotational degrees of freedom, respectively. [d]Assuming that at desorption temperature ΔG = 0 and $T\Delta S = \Delta H$

The results are summarized in Figure 4. As for the former case the black solid line is the experimental value[39] and the gray bar around it represents the chemical accuracy "region" around

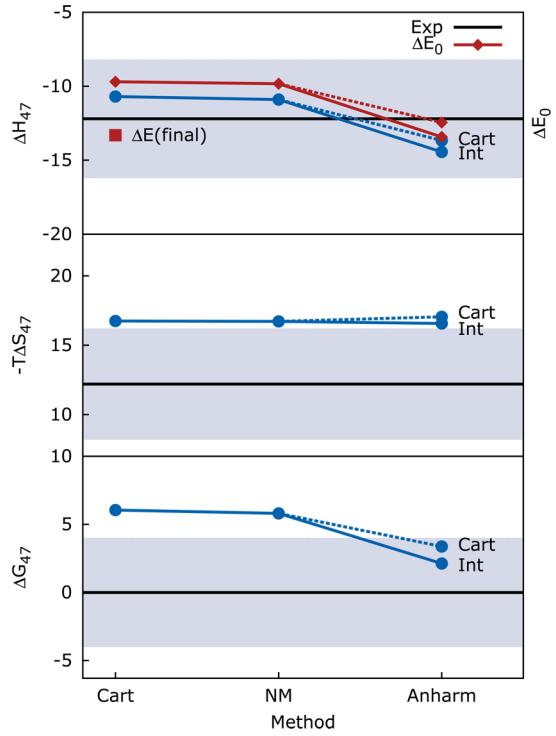

Figure 4. Enthalpies, ΔH, entropy, $-T\Delta S$, and Gibbs free energies, ΔG, for adsorption of methane on MgO(001) surface at experimental desorption conditions (47 K, 1.3×10^{-14} MPa, $\theta = 1$); all in kilojoules per mole (per molecule).

it. The red full square is the MP2:PBE+D + ΔCCSD(T) adsorption energy.

As for methane in H−CHA, the results obtained using anharmonic corrections with curvilinear displacements are in better agreement with the experimental results. It is very interesting that in this case it is the zero point vibrational energy and enthalpy change that makes the difference between the results for different methods, while the entropy term, due to the low temperature and pressure of the system, is not varying sensitively. The largest ZPV energy changes are associated with the anharmonic results obtained with curvilinear displacements. In this case the higher frequency modes make the largest contributions since they are drastically reduced by anharmonicity.

Since at low temperature and pressure, the energy changes are not as large as for standard conditions, the capability of the method can be better appreciated analyzing the variation of ΔG with the temperature. The desorption temperature is defined as $\Delta G(T) = 0$. Figure 5 shows the Gibbs free energy calculated using the different methods as a function of temperature. The black solid vertical line indicates the experimental desorption temperature (47 K).[39] It separates the temperature range for which the desorption is favored (gray region on its right) from the adsorption range.

The result obtained with anharmonic corrections using curvilinear displacements (44 K) shows very good agreement with the experimental desorption temperature (47 K). The Cartesian (Cart) and normal mode (NM) set of harmonic frequencies yield results that are very similar the one obtained by Tosoni and Sauer[45] (see Table 5). Table 5 reports also the desorption activation entropy barriers and prefactors. Here the entropy barrier is calculated taking the difference between the vibrational entropy of the adsorbed system and the vibrational

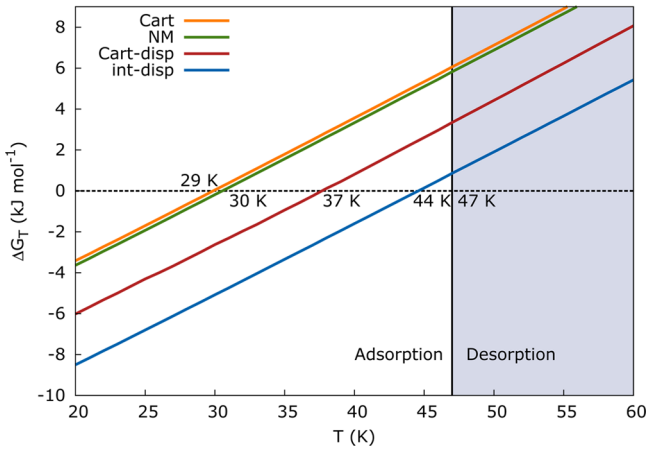

Figure 5. Variation of Gibbs free energy (kJ/mol) calculated using different methods with respect to temperature.

Table 5. Desorption Temperatures (K), T_{des}, Activation Entropy Barriers (J/K mol), $\Delta S^{\ddagger}$, and Decimal Logarithm of the Prefactors (s^{-1}), Log ν, for Adsorption of Methane on MgO(001) Calculated Using Different Methods

method		T_{des}	$\Delta S^{\ddagger}$	Log ν
Tosoni and Sauer[45]		33	−1.77[a]	12.02[a]
harmonic	Cart	29	−1.86	12.52
	NM	30	−2.00	12.53
anharmonic	Cart-disp	37	−2.10	12.59
	int-disp	44	−3.95	12.63
exp[39]		47		13.10

[a]Recalculated from the vibrational data of ref 45.

entropy of the same system for which the rigid perpendicular vibrations of the eight adsorbed methane molecules have been removed from the partition function[45] (one vibration per adsorbed CH_4 molecule). The latter are considered as the reaction coordinates in transition state theory when applied to the desorption process. Having this activation barrier, the prefactors are calculated as

$$\nu = \frac{k_B T}{h} e^{(1-\Delta S^{\ddagger}/R)} \tag{23}$$

where k_B is the Boltzmann constant, h is the Planck constant, and R is the molar gas constant. The prefactors calculated in this way are a common procedure in analyzing the temperature-programmed desorption (TPD) spectra, and they arise from the inversion of the Polanyi−Wigner equation for monomolecular desorption

$$-\alpha \frac{dN_a}{dT} = N_a \nu e^{-E_d^A/RT} \tag{24}$$

where N_a is the number of adsorbed molecules, T is the temperature which increases linearly with time t ($T = T_0 + \alpha t$), and E_d^A is the Arrhenius desorption energy.

As for the desorption temperature, the "anh-int" results show better agreement with the experimental data reported in ref 39.

CONCLUSIONS

The ab initio enthalpies, entropies, and free energies of adsorption calculated from vibrational partition functions using anharmonic corrections show agreement with the experimental data within chemical accuracy limits (4 kJ/mol) if curvilinear

dx.doi.org/10.1021/ct500291x | J. Chem. Theory Comput. 2014, 10, 2479−2487

displacements along normal modes are used. The proper sampling of the PES to get the one-dimensional anharmonic model potential proved to be essential for an accurate determination of thermodynamic functions. Simple harmonic frequencies, even when estimated with high accuracy (e.g., displacing the structure along normal modes if numerical derivatives are unavoidable), are not good enough to describe nonbonded interactions. As expected, anharmonic corrections enhance the vibrational entropy of the adsorption complex and, thus, favor adsorption.

For methane adsorption on Brønsted sites in zeolite H−CHA at standard conditions, anharmonicity changes the $T\Delta S$ term by as much as 18 kJ/mol, moving the equilibrium from desorption ($\theta = 9 \times 10^{-4}$) to adsorption ($\theta = 0.75$). For systems with very low desorption temperatures as methane on MgO(001), anharmonicity is found to cause significant changes on zero point vibrational energies and, thus, on the enthalpy as it lowers the higher vibrational wavenumbers. Anharmonicity effects change the adsorption energy at 0 K from 9.8 to 13.4 kJ/mol, and the heat of adsorption at 47 K from 10.9 to 14.4 kJ/mol. After inclusion of anharmonicity effects, the ab initio Gibbs free energies for adsorption of methane in H−CHA and methane on MgO(001) deviate by −3.6 and +2.1 kJ/mol, respectively, from the experimental data, showing that ab intio calculations yield Gibbs free energies within chemical accuracy limits.

■ ASSOCIATED CONTENT

Supporting Information

Solution of the anharmonic Hamiltonian, anharmonic vibrational thermodynamics functions, and refined structures employed in frequency calculations (VASP POSCAR format). This material is available free of charge via the Internet at http://pubs.acs.org/.

■ AUTHOR INFORMATION

Corresponding Author

*E-mail: piccingi@chemie.hu-berlin.de.

Notes

The authors declare no competing financial interest.

■ ACKNOWLEDGMENTS

This work has been supported by the "Fonds der Chemischen Industrie" and by a computer grant from the North German Computing Alliance Berlin—Hannover (HLRN). G.P. is a member of the International Max Planck Research School "Complex Surfaces in Material Sciences" and thanks the "Verband der Chemischen Industrie" for a Kekulé stipend. The authors acknowledge Drs. C. Tuma (Berlin) and A. Jentys (Vienna) for providing unpublished data. The authors would also like to specially acknowledge Prof. T. Bučko for valuable suggestions and for providing the Python script Write-Bmatrix.py which was crucial for the present work.

■ REFERENCES

(1) Claeyssens, F.; Harvey, J. N.; Manby, F. R.; Mata, R. A.; Mulholland, A. J.; Ranaghan, K. E.; Schütz, M.; Thiel, S.; Thiel, W.; Werner, H.-J. *Angew. Chem., Int. Ed.* **2006**, *45*, 6856−6859.
(2) Svelle, S.; Tuma, C.; Rozanska, X.; Kerber, T.; Sauer, J. *J. Am. Chem. Soc.* **2009**, *131*, 816−825.
(3) Hansen, N.; Kerber, T.; Sauer, J.; Bell, A. T.; Keil, F. J. *J. Am. Chem. Soc.* **2010**, *132*, 11525−11538.
(4) Tuma, C.; Sauer, J. *Angew. Chem., Int. Ed.* **2005**, *44*, 4769−4771.
(5) Bučko, T.; Benco, L.; Hafner, J.; Ángyán, J. G. *J. Catal.* **2007**, *250*, 171−183.
(6) Goltl, F.; Gruneis, A.; Bučko, T.; Hafner, J. *J. Chem. Phys.* **2012**, *137*, 114111.
(7) Sillar, K.; Hofmann, A.; Sauer, J. *J. Am. Chem. Soc.* **2009**, *131*, 4143−4150 PMID: 19253977.
(8) Sillar, K.; Sauer, J. *J. Am. Chem. Soc.* **2012**, *134*, 18354−18365.
(9) Sauer, J.; Sierka, M. *J. Comput. Chem.* **2000**, *21*, 1470−1493.
(10) De Moor, B. A.; Ghysels, A.; Reyniers, M.-F.; Van Speybroeck, V.; Waroquier, M.; Marin, G. B. *J. Chem. Theory Comput.* **2011**, *7*, 1090−1101.
(11) Campbell, C. T.; Sellers, J. R. V. *J. Am. Chem. Soc.* **2012**, *134*, 18109−18115.
(12) Rosta, E.; Klähn, M.; Warshel, A. *J. Phys. Chem. B* **2006**, *110*, 2934−2941.
(13) Hu, H.; Yang, W. *Annu. Rev. Phys. Chem.* **2008**, *59*, 573−601.
(14) Piccini, G.; Sauer, J. *J. Chem. Theory Comput.* **2013**, *9*, 5038−5045.
(15) Mace, A.; Laasonen, K.; Laaksonen, A. *Phys. Chem. Chem. Phys.* **2014**, *16*, 166−172.
(16) Torrie, G.; Valleau, J. *J. Comput. Phys.* **1977**, *23*, 187−199.
(17) Straatsma, T. P.; Berendsen, H. J. C. *J. Chem. Phys.* **1988**, *89*, 5876−5886.
(18) de Ruiter, A.; Oostenbrink, C. *J. Chem. Theory Comput.* **2012**, *8*, 3686−3695.
(19) Hobza, P.; Sauer, J.; Morgeneyer, C.; Hurych, J.; Zahradnik, R. *J. Phys. Chem.* **1981**, *85*, 4061−4067.
(20) De Moor, B. A.; Reyniers, M.-F.; Marin, G. B. *Phys. Chem. Chem. Phys.* **2009**, *11*, 2939−2958.
(21) De Moor, B. A.; Reyniers, M.-F.; Gobin, O. C.; Lercher, J. A.; Marin, G. B. *J. Phys. Chem. C* **2011**, *115*, 1204−1219.
(22) Cramer, C. J. *Essentials of computational chemistry: theories and models*; Wiley, 2004.
(23) Bouř, P.; Keiderling, T. A. *J. Chem. Phys.* **2002**, *117*, 4126−4132.
(24) Hudecová, J.; Hopmann, K. H.; Bouř, P. *J. Phys. Chem. B* **2012**, *116*, 336−342.
(25) Beste, A. *Chem. Phys. Lett.* **2010**, *493*, 200−205.
(26) Njegic, B.; Gordon, M. S. *J. Chem. Phys.* **2006**, *125*, 224102.
(27) De Silva, N.; Njegic, B.; Gordon, M. S. *J. Phys. Chem. A* **2011**, *115*, 3272−3278.
(28) De Silva, N.; Njegic, B.; Gordon, M. S. *J. Phys. Chem. A* **2012**, *116*, 12148−12152.
(29) Andzelm, J.; King-Smith, R.; Fitzgerald, G. *Chem. Phys. Lett.* **2001**, *335*, 321−326.
(30) Kudin, K. N.; Scuseria, G. E.; Schlegel, H. B. *J. Chem. Phys.* **2001**, *114*, 2919−2923.
(31) Bučko, T.; Hafner, J.; Ángyán, J. G. *J. Chem. Phys.* 2005, *122*, -.
(32) Barrer, R. M.; Davies, J. A. *Proc. R. Soc. London A* **1971**, *322*, 1−19.
(33) Corma, A. *Chem. Rev.* **1995**, *95*, 559−614.
(34) Eder, F.; Stockenhuber, M.; Lercher, J. A. *J. Phys. Chem. B* **1997**, *101*, 5414−5419.
(35) Papp, H.; Hinsen, W.; Do, N.; Baerns, M. *Thermochim. Acta* **1984**, *82*, 137−148.
(36) Sastre, F.; Fornés, V.; Corma, A.; Garca, H. *J. Am. Chem. Soc.* **2011**, *133*, 17257−17261.
(37) Smit, B.; Maesen, T. L. M. *Chem. Rev.* **2008**, *108*, 4125−4184.
(38) Wu, H.; Gong, Q.; Olson, D. H.; Li, J. *Chem. Rev.* **2012**, *112*, 836−868.
(39) Tait, S. L.; Dohnalek, Z.; Campbell, C. T.; Kay, B. D. *J. Chem. Phys.* **2005**, *122*, 164708.
(40) Jung, D. R.; Cui, J.; Frankl, D. R. *Phys. Rev. B* **1991**, *43*, 10042−10050.
(41) Larese, J. *Phys. B: Condensed Matter* **1998**, *248*, 297−303.
(42) Freitag, A.; Larese, J. Z. *Phys. Rev. B* **2000**, *62*, 8360−8365.
(43) Larese, J. Z.; y Marero, D. M.; Sivia, D. S.; Carlile, C. J. *Phys. Rev. Lett.* **2001**, *87*, 206102.

(44) Arnold, T.; Cook, R. E.; Chanaa, S.; Clarke, S. M.; Farinelli, M.; Yaron, P.; Larese, J. *Phys. B: Condensed Matter* **2006**, *385−386* (Part 1), 205−207.
(45) Tosoni, S.; Sauer, J. *Phys. Chem. Chem. Phys.* **2010**, *12*, 14330−14340.
(46) Njegic, B.; Gordon, M. S. *J. Chem. Phys.* **2008**, *129*, 164107.
(47) Bright Wilson, J. E.; Decius, J.; Cross, P. *Molecular Vibrations*; Dover Publishers, 1955.
(48) Bakken, V.; Helgaker, T. *J. Chem. Phys.* **2002**, *117*, 9160−9174.
(49) Boatz, J. A.; Gordon, M. S. *J. Phys. Chem.* **1989**, *93*, 1819−1826.
(50) Ayala, P. Y.; Schlegel, H. B. *J. Chem. Phys.* **1998**, *108*, 2314−2325.
(51) Konkoli, Z.; Cremer, D. *Int. J. Quantum Chem.* **1998**, *67*, 1−9.
(52) Konkoli, Z.; Larsson, J. A.; Cremer, D. *Int. J. Quantum Chem.* **1998**, *67*, 11−27.
(53) Konkoli, Z.; Cremer, D. *Int. J. Quantum Chem.* **1998**, *67*, 29−40.
(54) Konkoli, Z.; Larsson, J. A.; Cremer, D. *Int. J. Quantum Chem.* **1998**, *67*, 41−55.
(55) Jensen, F.; Palmer, D. S. *J. Chem. Theory Comput.* **2011**, *7*, 223−230.
(56) Baker, J.; Kessi, A.; Delley, B. *J. Chem. Phys.* **1996**, *105*, 192−212.
(57) Baker, J.; Pulay, P. *J. Chem. Phys.* **1996**, *105*, 11100−11107.
(58) Baker, J.; Kinghorn, D.; Pulay, P. *J. Chem. Phys.* **1999**, *110*, 4986−4991.
(59) Pulay, P.; Fogarasi, G. *J. Chem. Phys.* **1992**, *96*, 2856−2860.
(60) Kresse, G.; Hafner, J. *Phys. Rev. B* **1993**, *47*, 558−561.
(61) Perdew, J. P.; Chevary, J. A.; Vosko, S. H.; Jackson, K. A.; Pederson, M. R.; Singh, D. J.; Fiolhais, C. *Phys. Rev. B* **1992**, *46*, 6671.
(62) Grimme, S. *J. Comput. Chem.* **2006**, *27*, 1787−1799.
(63) Kerber, T.; Sierka, M.; Sauer, J. *J. Comput. Chem.* **2008**, *29*, 2088−2097.
(64) Monkhorst, H. J.; Pack, J. D. *Phys. Rev. B* **1976**, *13*, 5188−5192.
(65) Dove, M. T.; Harris, M. J.; Hannon, A. C.; Parker, J. M.; Swainson, I. P.; Gambhir, M. *Phys. Rev. Lett.* **1997**, *78*, 1070−1073.
(66) Hammonds, K. D.; Deng, H.; Heine, V.; Dove, M. T. *Phys. Rev. Lett.* **1997**, *78*, 3701−3704.
(67) Hammonds, K. D.; Heine, V.; Dove, M. T. *J. Phys. Chem. B* **1998**, *102*, 1759−1767.
(68) Dove, M. T.; Heine, V.; Hammonds, K. D. *Mineralog. Mag.* **1995**, *59*, 629−639.
(69) Fornberg, B. *Math. Comput.* **1988**, *51*, 699−706.
(70) Tuma, C.; Sauer, J. *Chem. Phys. Lett.* **2004**, *387*, 388−394.
(71) Tuma, C.; Sauer, J. *Phys. Chem. Chem. Phys.* **2006**, *8*, 3955−3965.
(72) Tuma, C.; Sauer, J. *unpublished results*, 2014.
(73) Tuma, C.; Kerber, T.; Sauer, J. *Angew. Chem.* **2010**, *49*, 4678−4690.
(74) Kolvenbach, R.; Jentys, A.; Lercher, J. A. *unpublished results*, 2014.